Analytical comparison between $X(3)$ and $X(5)$ models of the Bohr Hamiltonian

K.R. Ajulo[1]; **K.J. Oyewumi**[2]
[1,2]University of Ilorin, Ilorin, Nigeria.

Abstract

Via the inverse square potential, the solutions of the $X(3)$ model which is a γ-rigid form of the $X(5)$ critical point symmetry have been achieved. The paper presents $X(3)$, through the variational technique, as another "window" through which the "pictures" of $X(5) \longrightarrow SU(3)$ symmetry region can be seen. The analytical solutions of the $X(3)$ are compared with the solutions of the $X(5)$ model. Some new and unique equations connecting the two models in the: critical order, energy bands, spectra ratios, $R_{L/2}$, and $B(E2)$ transitional probabilities are presented. These equations should hold in other potentials with one-parameter such as Kratzer potential, Davidson potential etc. The spectra ratios and the $B(E2)$ transitional probabilities are optimized via the optimization procedure. The experimental data of some selected isotopes are placed accordingly for the theoretical predictions. The deviations from the experiments are found to be quite small.

Keywords: Bohr Hamiltonian, $X(3)$, $X(5)$, variation technique, optimization procedure, β-variable, γ-rigid.

arXiv:2301.00533v1 [nucl-th] 2 Jan 2023

1 Introduction

$X(3)$ which has been presented in [1-4] is said to be an exactly separable γ-rigid form of the $X(5)$ critical point symmetry [5]. The $X(3)$ model is defined by the collective coordinate β and two Euler angles since the γ is assumed to be zero unlike the case of $X(5)$, where γ is varied around $\gamma^0 = 0$ value in the harmonic oscillator potential [5]. This implies that, only three variables: β and θ_i are involved in the $X(3)$ model. An exact separation of the β variable from the Euler angles is quite easily achievable. In the Bohr Hamiltonian model [6-9], $X(5)$ critical point symmetry is one of the two critical point symmetries: it is a phase transition of the first order shape, which were originally proposed in the works of Iachello [10], while $E(5)$ is the phase transition of the second order shape [10]. In the present work, the nuclei are taken to be γ-rigid, with the axially symmetric prolate shape obtained at $\gamma^0 = 0$. The work presents the usefulness of a one-sided bound inverse square potential with one parameter. The one-parameter inverse square potential chosen is of the form

$$V(\beta) = \begin{cases} \dfrac{\beta_0}{\beta^2}, \text{ if } 0 \leq \beta \leq \beta_0, \\ \infty, \text{ if } \beta > \beta_0, \end{cases} \tag{1}$$

where β_0 is a variation parameter that changes the signatures of the nuclei, as it changes. It is expected that the solutions should shift forward as the β_0 shifts forward and solutions should shift backward as the β_0 shifts backward. A typical inverse square potential is bound on the left and unbound on the right, and it has a minimum at some positive values of β_0 that forces the particles to infinity as $\beta_0 \to 0$. As a result, the particle's energy states is one-sided, with energies escaping through the unbound side. The work is structured as follows: Section 2. presents the methodology and the solutions of $X(3)$ model via inverse square potential. These solutions are: the wave functions, the normalization constants and the energy eigenvalues. The $B(E2)$ transition rates are presented in Section 3. The analytical results, the numerical results, their applications in certain isotopes are presented and discussed in Section 4. The work is concluded and summarized in the Section 5.

[1]E-Mail: 19-68eo001@students.unilorin.edu.ng
[2]E-Mail: kjoyewumi66@unilorin.edu.ng

2 Methodology of $X(3)$ model with the inverse square potential

In the $X(3)$ model, the Bohr Hamiltonian operator is written as [1,2]

$$\hat{H} = -\frac{\hbar^2}{2B}\left[\frac{1}{\beta^2}\frac{\partial}{\partial\beta}\beta^2\frac{\partial}{\partial\beta} + \frac{1}{3\beta^2}\left(\frac{1}{\sin\theta}\frac{\partial}{\partial\theta}\sin\theta\frac{\partial}{\partial\theta} + \frac{1}{\sin^2\theta}\frac{\partial^2}{\partial\phi^2}\right) - V(\beta)\right], \tag{2}$$

where the term,

$$\frac{1}{\sin\theta}\frac{\partial}{\partial\theta}\sin\theta\frac{\partial}{\partial\theta} + \frac{1}{\sin^2\theta}\frac{\partial^2}{\partial\phi^2}, \tag{3}$$

inside the bracket, represents the angular part of the Laplacian [1,2] . B, β and $V(\beta)$ are respectively the mass parameter, the collective coordinate and the β-dependent potential. The wave equation of the Eq.(2) is

$$\hat{H}\Psi(\beta,\theta,\phi) = E\Psi(\beta,\theta,\phi). \tag{4}$$

By the usual method of separation of variable employed in some quantum texts,

$$\Psi(\beta,\theta,\phi) = \chi(\beta)Y_{L,M}(\theta,\phi), \tag{5}$$

where $Y_{L,M}(\theta,\phi)$ is the spherical harmonics and $\chi(\beta)$ is the radial part of Eq.(4). The separated angular part obtained reads [1,2]

$$-\left(\frac{1}{\sin\theta}\frac{\partial}{\partial\theta}\sin\theta\frac{\partial}{\partial\theta} + \frac{1}{\sin^2\theta}\frac{\partial^2}{\partial\phi^2}\right)Y_{L,M}(\theta,\phi) = L(L+1)Y_{L,M}(\theta,\phi), \tag{6}$$

where L is the angular momentum quantum number. The simplified form of the radial part equation [1,2] ,

$$\left(\frac{1}{\beta^2}\frac{d}{d\beta}\beta^2\frac{d}{d\beta} - \frac{L(L+1)}{3\beta^2} + \frac{2B}{\hbar^2}[E - V(\beta)]\right)\chi(\beta) = 0 \tag{7}$$

reads

$$\frac{d^2}{d\beta^2}\chi(\beta) + \frac{2}{\beta}\frac{d}{d\beta}\chi(\beta) - \frac{L(L+1)}{3\beta^2}\chi(\beta) - [v(\beta) - \epsilon]\chi(\beta) = 0, \tag{8}$$

where $\epsilon = \frac{2B}{\hbar^2}E$ and $v(\beta) = \frac{2B}{\hbar^2}V(\beta)$ are the reduced energy and reduced potential respectively [5].

2.1 Determination of the wave functions

By substituting Eq.(1) for $v(\beta)$ in Eq.(8) and solving the simplified equation using MAPLE software, the eigenfunctions obtained read

$$\chi_{s,\nu,L,}(\beta) = \beta^{-1/2}\left[C_{1,L}J_\nu(\sqrt{\epsilon}\beta) + C_{2,L}Y_\nu(\sqrt{\epsilon}\beta)\right], \tag{9}$$

where $C_{1,L}$ and $C_{2,L}$ are the normalization constants associated with the Bessel functions of the first kind, J_ν, and second kind, Y_ν, respectively. In the domain of Eq.(1), the critical order associated with the $X(3)$ model in Eq.(9) is

$$\nu^{X(3)} = \sqrt{\frac{L}{3}(L+1) + \beta_0 + \frac{1}{4}}. \tag{10}$$

If a boundary condition $\chi_{s,\nu,L}(\beta_0) = 0$ is considered, then $C_{2,L,n}Y_\nu(\sqrt{\epsilon}\beta)$ vanishes and the wave functions become

$$\chi_{s,\nu,L}(\beta) = \beta^{-1/2}\left[C_{1,L}J_\nu(\sqrt{\epsilon}\beta)\right]. \tag{11}$$

2.2 Determination of the energy eigenvalues and the spectral ratio

The procedure for finding the eigenvalues is written in ref. [11]. If the first condition of the listed procedure is considered, then the acceptable expression for the energy eigenvalues is written as:

$$E_{s,L,n_\beta} = \frac{\hbar^2}{2B} k^2_{s,\nu,n_\beta}, \quad k^2_{s,\nu,n_\beta} = \epsilon_{s,\nu,n_\beta}, \quad k^2_{s,\nu,n_\beta} = \frac{x_{n_\beta,s,\nu}}{\beta_0}, \tag{12}$$

where $s = n_\beta + 1$, x_{s,ν,n_β} is the s-th zeros of the Bessel function of order ν. The energy eigenvalues of the β-part in $\hbar\omega = 1$ unit reads:

$$\epsilon_{s,L,n_\beta} = 2n_\beta + 1 + \nu^{X(3)} = 2n_\beta + 1 + \sqrt{\frac{L}{3}(L+1) + \beta_0 + \frac{1}{4}} : \quad n_\beta = 0, 1, 2, ... \tag{13}$$

For the $X(3)$ model, the ground state energy levels are defined with $s = 1$, the quasi-β_1 levels are defined with $s = 2$ and the quasi-β_2 levels are defined with $s = 3$. $L = 0, 2, 4, 6...$ There exist no γ-bands in the $X(3)$ model because, $\gamma^0 = 0$.
Eq.(13) is the similar to the energy eigenvalues obtained in the β-part of $X(5)$ model [12], the difference is observed in their critical orders where

$$\nu^{X(5)} = \sqrt{\frac{L}{3}(L+1) + \beta_0 + \frac{9}{4}}. \tag{14}$$

Since $s = n_\beta + 1$, ϵ_{s,L,n_β} can be reduced to $\epsilon_{s,L}$, then the spectra ratios can be written as

$$R_{L/2} = \frac{\epsilon_{s,L} - \epsilon_{1,0}}{\epsilon_{1,2} - \epsilon_{1,0}}. \tag{15}$$

2.3 Determination of the normalization constants and the complete wave functions

The normalization condition for the Hamiltonian operator in Eq.(2) is written as [1,2]

$$\int_0^{\beta_0} \beta^2 \mid \chi_{s,\nu,L,n_\beta}(\beta) \mid^2 d\beta = 1, \tag{16}$$

such that

$$\mid \chi_{s,\nu,L,n_\beta}(\beta) \mid^2 \to 0 \quad \text{for} \quad \beta \to 0; \quad \mid \chi_{s,\nu,L,n_\beta}(\beta) \mid^2 \beta^2 \to 0 \quad \text{for} \quad \beta \to \infty. \tag{17}$$

If these conditions are satisfied, then $\int_0^{\beta_0} \beta^2 \mid \chi_{s,\nu,L,n_\beta}(\beta) \mid^2 d\beta < \beta_0$.
Using the identity [13-14]

$$J_\nu(\sqrt{\epsilon}\beta) J_\nu(\sqrt{\epsilon}\beta) = \sum_{n_\beta=0}^{\infty} \frac{\left(\frac{1}{2}\sqrt{\epsilon}\beta\right)^{2\nu+2n_\beta} (2\nu + n_\beta + 1)_{n_\beta}}{n_\beta![\Gamma(\nu + n_\beta + 1)]^2} \tag{18}$$

in Eq.(16), the simplified normalization constants read

$$C_{1,L,n_\beta} = \left[\sum_{n_\beta=0,1,2,3...} \frac{(\eta)_{n_\beta} \left(\frac{k_{s,\nu,n_\beta}}{2}\right)^{\xi-2} \beta_0^{(\xi)}}{n_\beta! \quad \xi \quad \left[\Gamma\left(\frac{\xi}{2}\right)\right]^2} \right]^{-1/2}, \tag{19}$$

where

$$\xi = 2\nu + 2n_\beta + 2, \quad \eta = 2\nu + n_\beta + 1 \quad \text{and} \quad (\eta)_{n_\beta} = \eta(\eta+1)(\eta+2)...(\eta + n_\beta - 1), \tag{20}$$

with $(\eta)_0 = 1$. Hence, Eq.(11) becomes

$$\chi_{s,\nu,L,n_\beta}(\beta) = \left[\sum_{n_\beta=0,1,2,3...} \frac{(\eta)_{n_\beta} \left(\frac{k_{s,\nu,n_\beta}}{2}\right)^{\xi-2} \beta_0^{(\xi)}}{n_\beta! \quad \xi \quad \left[\Gamma\left(\frac{\xi}{2}\right)\right]^2} \right]^{-1/2} \beta^{-1/2} J_\nu(\sqrt{\epsilon}\beta). \tag{21}$$

3 $B(E2)$ transition rates

The electric quadrupole operator is written as [1,2]

$$T^{E2}_\mu = t\beta \left[D^{(2)}_{\mu,0}(\theta_i)\cos\gamma + \frac{1}{\sqrt{2}}\left(D^{(2)}_{\mu,2}(\theta_i) + D^{(2)}_{\mu,-2}(\theta_i)\right)\sin\gamma \right], \tag{22}$$

where $D(\theta_i)$ are the Wigner functions of the Euler angle and t is known as a scale factor. For $\gamma^0 = 0$,

$$T^{E2}_\mu = t\beta\sqrt{\frac{4\pi}{5}} Y_{2\mu}(\theta,\phi). \tag{23}$$

The $B(E2)$ [1,2,5,15] is written as

$$B(E2; sL \longrightarrow s'L') = \frac{1}{2sL+1} |\left\langle s'L' || T^{E2} || sL \right\rangle|^2, \tag{24}$$

$$= \frac{2s'L'+1}{2sL+1} B(E2; s'L' \longrightarrow sL). \tag{25}$$

Eq.(24) or Eq.(25) has been solved in ref. [1] as:

$$B(E2; sL \longrightarrow s'L') = t^2 \left(C^{L'0}_{L0,20}\right)^2 I^2_{sL;s'L'}, \tag{26}$$

where the coefficients, $C^{L'0}_{L0,20}$ are the Clebsch-Gordan coefficients, and

$$I_{sL;s'L'} = \int_0^{\beta_0} \beta \chi_{s,\nu,L,n_\beta}(\beta) \chi_{s',\nu',L',n'_\beta}(\beta) \beta^2 d\beta, \tag{27}$$

are the integrals over β.

4 Numerical results, analytical results, applications and discussion

Some important solutions for the collective model of Eq.(2) are the energy levels, the spectra ratios and the $B(E2)$ transitions. Their theoretical predictions are important when energy spectra are assigned to the states for which experimental data are not available. The numerical calculations, the analytical comparisons and how the search for the experimental realizations of the model was achieved are discussed accordingly in this section.

Both the $X(3)$ and the $X(5)$ have their critical orders, $\nu(L,\beta_0)$, from their Bessel functions which describes their energy spectra. Firstly, in the comparison of the Eq.(10) and Eq.(14), it can be deduced from the numerical computation of ν, shown in Table 1., that

$$\nu^{X(3)}(\beta_0 = c+2) = \nu^{X(5)}(\beta_0 = c): \quad c = 0,1,2,... \tag{28}$$

In both cases, it increases with increase in the angular momentum, L, and with increase in the variation parameter, β_0. These effects of L and β_0 in ν are also seen in the energy values of Eq.(13).

Table 1: The comparison in the critical order, ν, of the $X(5)$ [12], with the ν of Eq.(10).

	$\nu(L)$									
L	$\beta_0=0$		$\beta_0=2$		$\beta_0=4$		$\beta_0=6$		$\beta_0=102$	$\beta_0=100$
	$X(3)$	$X(5)$	$X(3)$	$X(5)$	$X(3)$	$X(5)$	$X(3)$	$X(5)$	$X(3)$	$X(5)$
0	0.500	1.500	1.500	2.062	2.062	2.500	2.500	2.062	10.112	10.112
2	1.500	2.062	2.062	2.500	2.500	2.872	2.872	2.500	10.210	10.210
4	2.630	2.986	2.986	3.304	3.304	3.594	3.594	3.304	10.436	10.436
6	3.775	4.031	4.031	4.272	4.272	4.500	4.500	4.272	10.782	10.782
8	4.924	5.123	5.123	5.315	5.315	5.500	5.500	5.315	11.236	11.236
10	6.076	6.238	6.238	6.397	6.397	6.551	6.551	6.397	11.786	11.786
	$\beta_0=1$		$\beta_0=3$		$\beta_0=5$		$\beta_0=7$		$\beta_0=101$	$\beta_0=103$
0	1.118	1.803	1.803	2.291	2.291	2.693	2.693	3.041	10.062	10.259
2	1.803	2.291	2.291	2.693	2.693	3.041	3.041	3.354	10.161	10.356
4	2.814	3.149	3.149	3.452	3.452	3.731	3.731	3.990	10.388	10.579
6	3.905	4.153	4.153	4.387	4.387	4.610	4.610	4.823	10.735	10.920
8	5.025	5.220	5.220	5.408	5.408	5.590	5.590	5.766	11.191	11.369
10	6.158	6.318	6.318	6.474	6.474	6.627	6.627	6.776	11.747	11.913

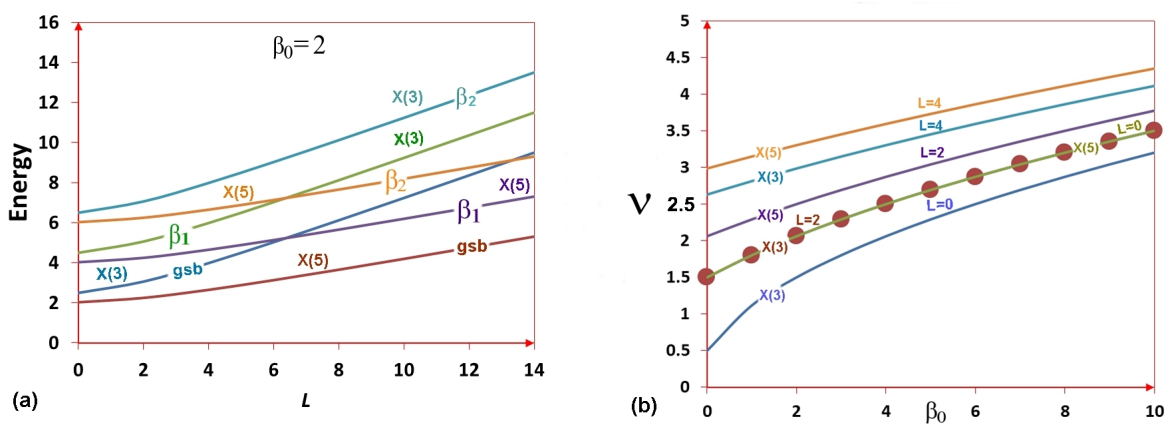

Figure 1: (a) Comparison in the energy levels of the $X(3)$ and $X(5)$ models [15] at $\beta_0=2$ from the gsb up to the quasi-β_2 band. (b): the variation of the critical order, ν, of the $X(5)$ as a function of β_0, is compared with ν of the $X(3)$ at constant angular momenta, $L=0,2$ and $L=4$.

Table 2: Ground state energies, the energies of the quasi-β_1 and the quasi-β_2 denoted by $n_\beta = 0, s = 1$; $n_\beta = 1, s = 2$; and $n_\beta = 2, s = 3$ respectively for the $X(3)$ and $X(5)$ symmetry [12] in $\hbar\omega = 1$ unit.

	$\beta_0 = 2$		$\beta_0 = 3$		$\beta_0 = 4$		$\beta_0 = 15$	
L					$n_\beta = 0;$ $s = 1$			
	$X(3)$	$X(5)$	$X(3)$	$X(5)$	$X(3)$	$X(5)$	$X(3)$	$X(5)$
0	2.500	2.031	2.803	2.146	3.062	2.250	4.905	3.077
2	3.062	2.250	3.291	2.346	3.500	2.436	5.153	3.194
4	3.986	2.652	4.149	2.726	4.304	2.797	5.682	3.445
6	5.031	3.136	5.153	3.194	5.272	3.250	6.408	3.795
8	6.123	3.658	6.220	3.704	6.315	3.750	7.265	4.212
10	7.238	4.198	7.318	4.237	7.397	4.276	8.205	4.671
12	8.365	4.750	8.433	4.783	8.500	4.816	9.201	5.161
14	9.500	5.308	9.559	5.337	9.617	5.366	10.233	5.670
					$n_\beta = 1;$ $s = 2$			
0	4.500	4.031	4.803	4.146	5.062	4.250	6.905	5.077
2	5.062	4.250	5.291	4.346	5.500	4.436	7.153	5.194
4	5.986	4.652	6.149	4.726	6.304	4.797	7.682	5.445
6	7.031	5.136	7.153	5.194	7.272	5.250	8.408	5.795
8	8.123	5.658	8.220	5.704	8.315	5.750	9.265	6.211
10	9.238	6.198	9.318	6.237	9.397	6.276	10.205	6.671
12	10.365	6.750	10.433	6.783	10.500	6.816	11.201	7.161
14	11.500	7.308	11.559	7.337	11.617	7.366	12.233	7.670
					$n_\beta = 2;$ $s = 3$			
0	6.500	6.031	6.803	6.146	7.062	6.250	8.905	7.077
2	7.062	6.250	7.291	6.346	7.500	6.436	9.153	7.194
4	7.986	6.652	8.149	6.726	8.304	6.797	9.682	7.445
6	9.031	7.136	9.153	7.194	9.272	7.250	10.408	7.795
8	10.123	7.658	10.220	7.704	10.315	7.750	11.265	8.211
10	11.238	8.198	11.318	8.237	11.397	8.276	12.205	8.671
12	12.365	8.750	12.433	8.783	12.500	8.816	13.201	9.161
14	13.500	9.308	13.559	9.337	13.617	9.366	14.233	9.670

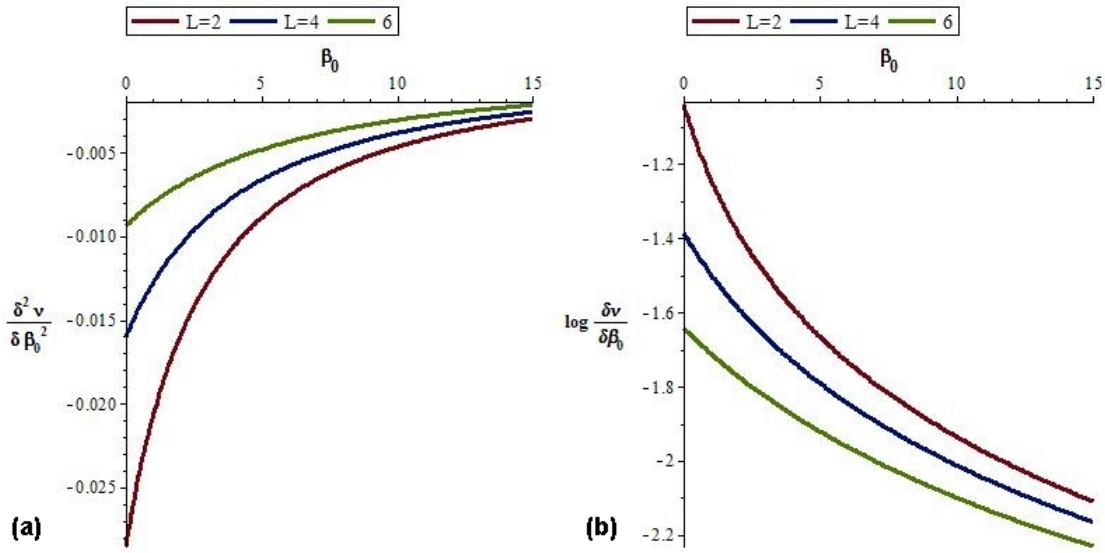

Figure 2: (a) The plots showing the values of β_0 at which energies are minimum. (b) The rate of energy with respect to β_0, showing non stationary property of β_0.

Table 3: Comparison of the ground state spectra ratios, defined in Eq.(15), of the inverse square potential in the $X(3)$ model at different values of the β_0, compared with the $X(5)$ [12]. It can be seen that $X(3)(\beta_0 = \infty) \approx X(5)(\beta_0 = \infty)$.

L_{s,n_β}	$\beta_0 = 0$	$\beta_0 = 0$	$\beta_0 = 2$	$\beta_0 = 2$	$\beta_0 = 4$	$\beta_0 = 4$	$\beta_0 = \infty$	$\beta_0 = \infty$
	$X(3)$	$X(5)$	$X(3)$	$X(5)$	$X(3)$	$X(5)$	$X(3)$	$X(5)$
gsb								
$0_{1,0}$	0.000	0.000	0.000	0.000	0.000	0.000	0.000	0.000
$2_{1,0}$	1.000	1.000	1.000	1.000	1.000	1.000	1.000	1.000
$4_{1,0}$	2.130	2.646	2.646	2.834	2.834	2.938	3.296	3.296
$6_{1,0}$	3.275	4.507	4.507	5.042	5.042	5.372	6.806	6.808
$8_{1,0}$	4.424	6.453	6.453	7.421	7.421	8.508	11.413	11.423
$10_{1,0}$	5.576	8.438	8.438	9.887	9.887	11.881	16.991	17.013
$12_{1,0}$	6.728	10.445	10.445	12.404	12.404	15.686	23.409	23.450
$14_{1,0}$	7.882	12.465	12.465	14.951	14.951	19.740	30.544	30.611
	$\beta_0 = 1$	$\beta_0 = 1$	$\beta_0 = 3$	$\beta_0 = 3$	$\beta_0 = 5$	$\beta_0 = 5$	$\beta_0 = 15$	$\beta_0 = 15$
$0_{1,0}$	0.000	0.000	0.000	0.000	0.000	0.000	0.000	0.000
$2_{1,0}$	1.000	1.000	1.000	1.000	1.000	1.000	1.000	1.000
$4_{1,0}$	2.476	2.756	2.756	2.893	2.893	2.946	3.128	3.148
$6_{1,0}$	4.070	4.812	4.812	5.224	5.224	5.529	6.058	6.136
$8_{1,0}$	5.706	6.995	6.995	7.767	7.767	8.638	9.508	9.690
$10_{1,0}$	7.360	9.243	9.243	10.424	10.424	11.915	13.297	13.620
$12_{1,0}$	9.024	11.525	11.525	13.145	13.145	15.854	17.307	17.800
$14_{1,0}$	10.694	13.829	13.829	15.907	15.907	19.899	21.468	22.152

Table 4: $R_{L/2}$ ratios, defined in Eq.(15), of the quasi-β_1 and quasi-β_2 bands of the inverse square potential in the $X(3)$ model at different values of the β_0.

L_{s,n_β}	$\beta_0=0$	$\beta_0=1$	$\beta_0=2$	$\beta_0=3$	$\beta_0=4$	$\beta_0=15$	$\beta_0=\infty$
quasi-β_1							
$0_{2,1}$	2.000	2.921	3.562	4.094	4.562	8.058	20.124
$2_{2,1}$	3.000	3.921	4.562	5.094	5.562	9.058	21.124
$4_{2,1}$	4.130	5.397	6.208	6.850	7.395	11.187	23.420
$6_{2,1}$	5.275	6.991	8.069	8.906	9.603	14.115	26.929
$8_{2,1}$	6.424	8.626	10.014	11.090	11.982	17.567	31.537
$10_{2,1}$	7.576	10.281	11.999	13.337	14.449	21.356	37.116
$12_{2,1}$	8.728	11.945	14.007	15.619	16.965	25.366	43.534
$14_{2,1}$	9.882	13.615	16.027	17.923	19.513	29.526	50.668
quasi-β_2							
$0_{3,2}$	4.000	5.842	7.123	8.188	9.123	16.117	40.249
$2_{3,2}$	5.000	6.842	8.123	9.188	10.123	17.117	41.249
$4_{3,2}$	6.130	8.318	9.769	10.944	11.957	19.245	43.545
$6_{3,2}$	7.275	9.912	11.630	13.000	14.165	22.174	47.054
$8_{3,2}$	8.424	11.547	13.576	15.184	16.544	25.625	51.662
$10_{3,2}$	9.576	13.201	15.561	17.431	19.010	29.414	57.240
$12_{3,2}$	10.728	14.866	17.568	19.713	21.527	33.424	63.658
$14_{3,2}$	11.882	16.536	19.589	22.018	24.074	37.584	70.792

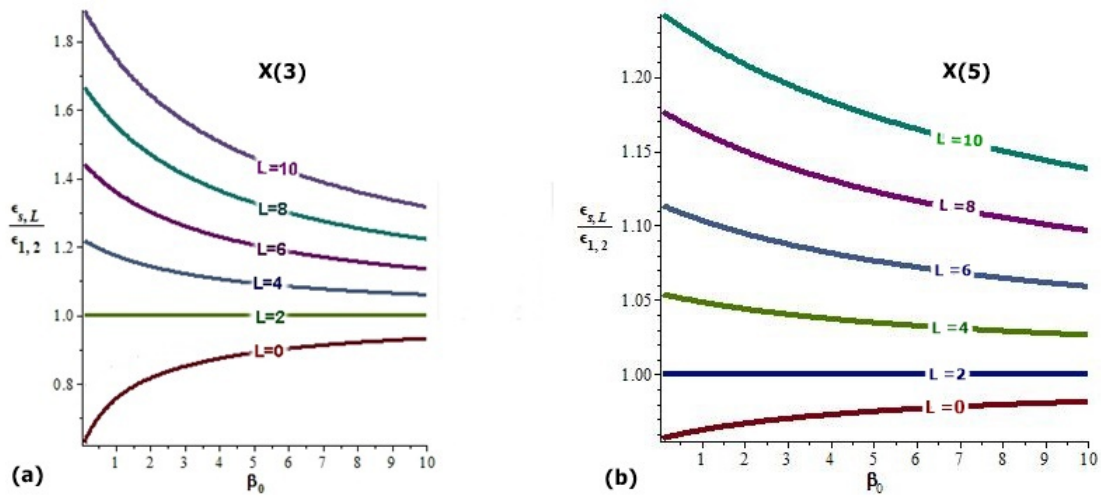

Figure 3: The $\frac{\epsilon_{s,L}}{\epsilon_{1,2}}$ of the $X(3)$. (b): the $\frac{\epsilon_{s,L}}{\epsilon_{1,2}}$ of the $X(5)$ both at constant angular momenta, $L=0...10$ are plotted against the variation parameter, β_0.

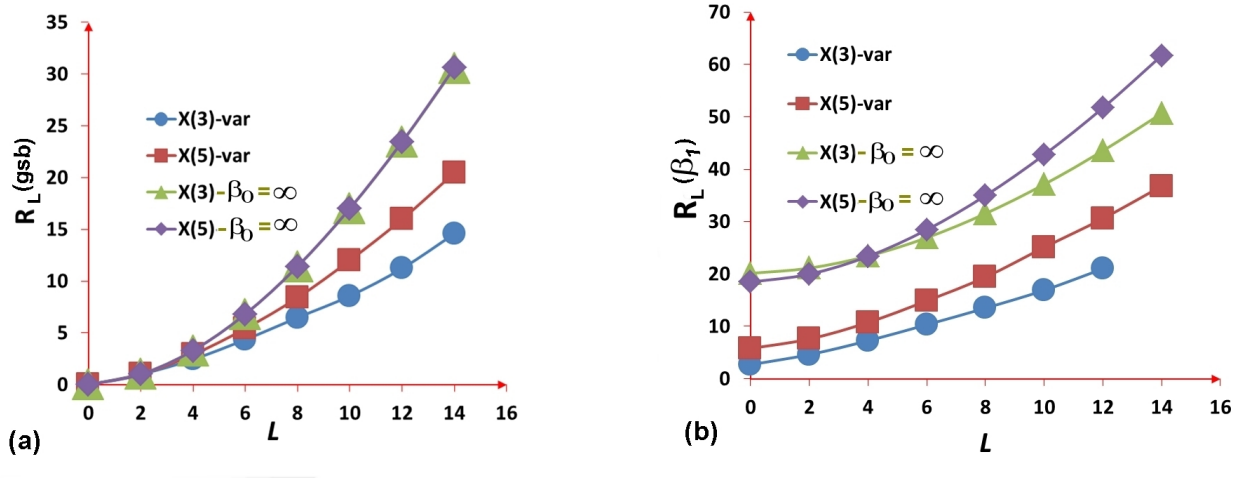

Figure 4: (a) The comparison in the $R_{4/2}$ of the $X(3)$ and $X(5)$ for $\beta_0 = \infty$ and for different values of the $\beta_{0,max}$ labelled as $X(3)-$var and $X(5)-$var respectively, peculiar to each angular momentum. (b): the comparison in the $R_{0/2}$ of the $X(3)$ and $X(5)$ for $\beta_0 = \infty$ and for different values of the $\beta_{0,max}$ labelled as $X(3)-$var and $X(5)-$var respectively, peculiar to each angular momentum.

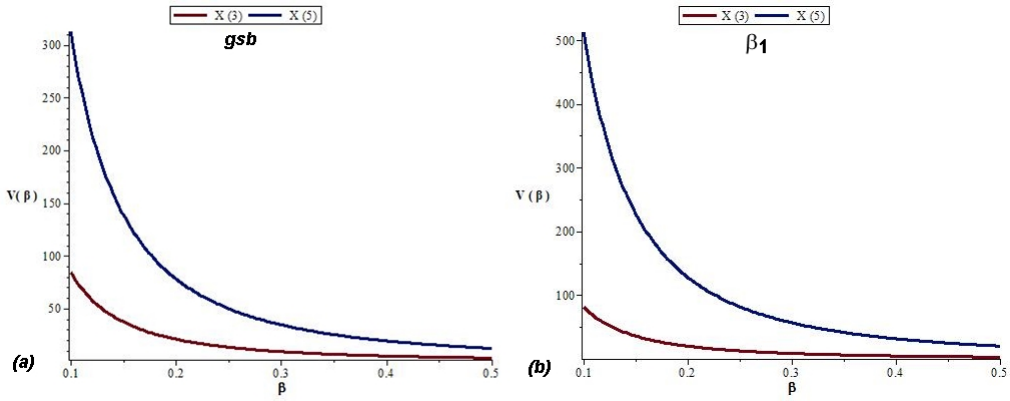

Figure 5: (a) and (b) The visual plots of the potentials correspond to $R_{4/2}$ and $R_{0/2}$ respectively. The values of β_0 used correspond to $X(3)$-var and $X(5)$-var in the gsb and quasi-β_1 bands.

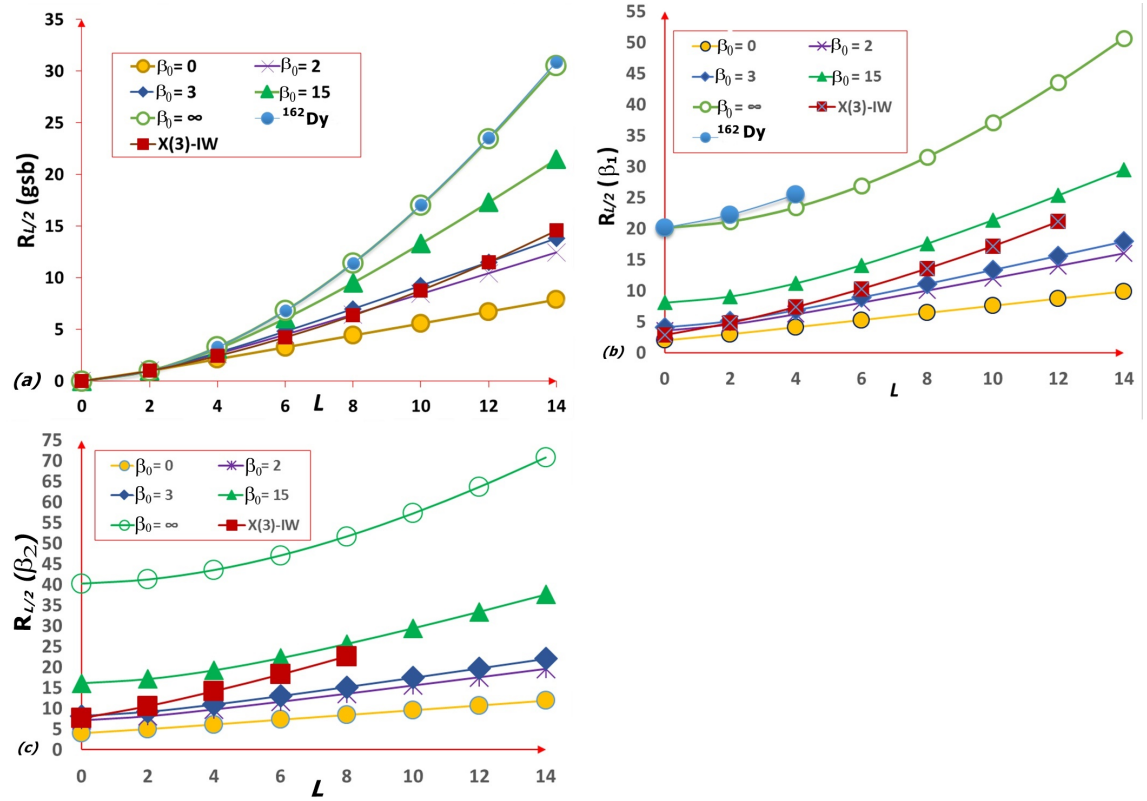

Figure 6: (a) and (b) present the $R_{L/2}$ ratios for the ground state and the quasi-β_1 bands of the $X(3)$ model of inverse square potential respectively, at different values of β_0 compared with $X(3)$-IW and ^{162}Dy. (c): the $R_{L/2}$ ratios for the quasi-β_2 bands of the $X(3)$ model of inverse square potential at different values of β_0 compared with $X(3)$-IW [1]. It appears that the *gsb* solutions of $X(3)$ at $\beta_0 = \infty$ lie on the experimental data of ^{162}Dy, which is a typical $SU(3)$ candidate. The available data on the first exited state lie very close to one another.

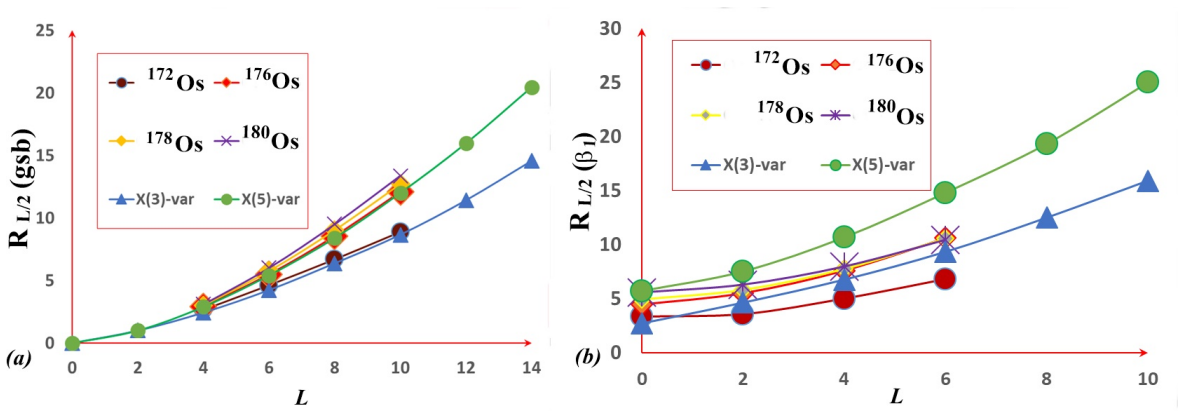

Figure 7: (a) and (b) present the $R_{L/2}$ ratios for the ground state and the quasi-β_1 bands of the $X(3)$ and the $X(5)$ models of inverse square potentials respectively, obtained at different values of $\beta_{0,max}$, labeled $X(3)$-var and $X(5)$-var, are compared with the $^{172-180}$Os chain.

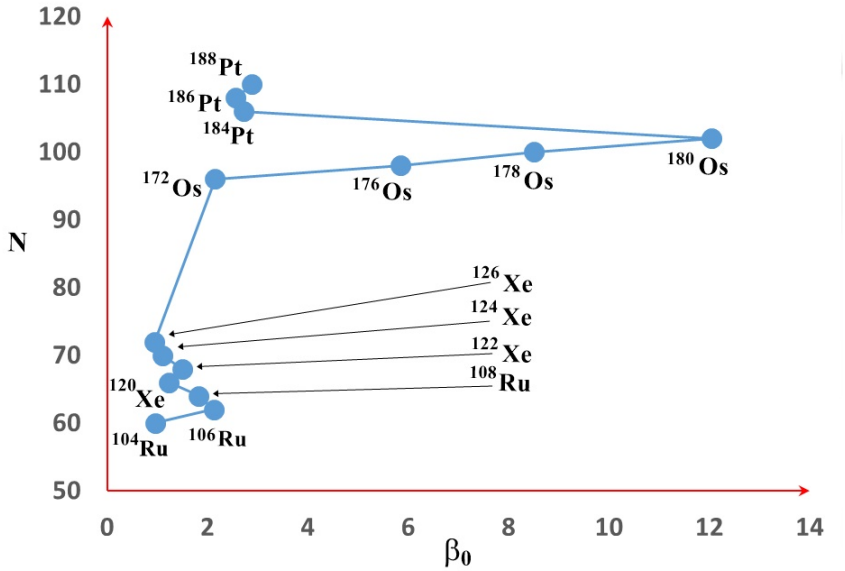

Figure 8: The Neutron-β_0 distribution is employed to show the relative positions of $^{104-108}$Ru, $^{120-126}$Xe, $^{184-188}$Pt and $^{172-180}$Os along their common chain.

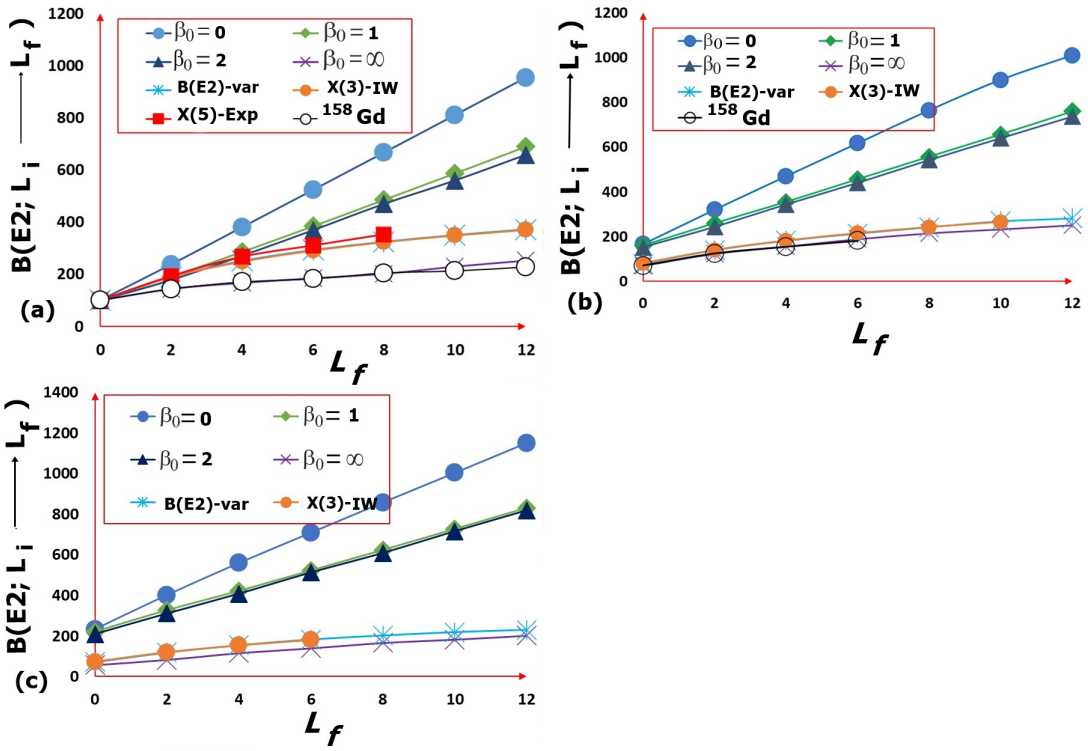

Figure 9: The $B(E2)$ transition rates of the $X(3)$ normalized to the $B(E2: 2_{1,0} \to 0_{1,0}) = 100$ units within: (a) the ground state bands at $\beta_0 = 0, 1, 2, \infty$ and $B(E2)$-var compared with the $X(3)$-IW [1], $X(5)$ experimental data [34] and ^{158}Gd [35], which is a typical $SU(3)$ candidate. (b): the β_1 state bands at $\beta_0 = 0, 1, 2, \infty$ and $B(E2)$-var compared with the $X(3)$-IW [1] and ^{158}Gd. (c): the β_2 state bands at $\beta_0 = 0, 1, 2, \infty$ and $B(E2)$-var compared with the $X(3)$-IW [1]. [Note:-IW denotes infinite well potential.]

Table 5: The $R_{L/2}$ ratios, defined in Eq.(15), for the $X(3)$ version of inverse square potential, labelled $X(3)$-var, calculated at different values of $\beta_{0,max}$, are compared with the $X(3)$-IW [1]. [Note: IW denotes infinite well potential].

L_{s,n_β}	$\beta_{0,max}$	$X(3)$-var	$X(3)$-IW
gsb			
$0_{1,0}$	β_0	0.000	0.000
$2_{1,0}$	β_0	1.000	1.000
$4_{1,0}$	0.844	2.440	2.440
$6_{1,0}$	1.576	4.244	4.230
$8_{1,0}$	2.033	6.383	6.350
$10_{1,0}$	2.143	8.666	8.780
$12_{1,0}$	2.695	11.421	11.520
$14_{1,0}$	3.643	14.573	14.570
quasi-β_1			
$0_{2,1}$	0.815	2.703	2.870
$2_{2,1}$	2.101	4.619	4.830
$4_{2,1}$	3.729	7.255	7.370
$6_{2,1}$	5.213	10.327	10.290
$8_{2,1}$	6.098	13.493	13.570
$10_{2,1}$	6.855	16.908	17.180
$12_{2,1}$	8.106	21.009	21.140
quasi-β_2			
$0_{3,2}$	2.524	7.701	7.650
$2_{3,2}$	4.497	10.553	10.560
$4_{3,2}$	6.523	14.088	14.190
$6_{3,2}$	8.567	18.172	18.220
$8_{3,2}$	10.438	22.613	22.620
$10_{3,2}$	11.932	25.999	-
$12_{3,2}$	13.011	28.928	-

Table 6: The spectra ratios for the $X(3)$ version of inverse square potential are compared with the experimental data. The values of the β_0 and the quality factor, σ, used during the fittings are recorded.

L_{s,n_β}	^{102}Mo Exp	^{102}Mo Theor	^{104}Ru Exp	^{104}Ru Theor	^{106}Ru Exp	^{106}Ru Theor	^{108}Ru Exp	^{108}Ru Theor	^{120}Xe Exp	^{120}Xe Theor	^{122}Xe Exp	^{122}Xe
gsb												
$4_{1,0}$	2.510	2.566	2.480	2.468	2.660	2.662	2.750	2.623	2.470	2.522	2.500	2.571
$6_{1,0}$	4.480	4.483	4.350	4.299	4.800	4.805	5.120	5.102	4.330	4.263	4.430	4.500
$8_{1,0}$	6.810	6.703	6.480	6.488	7.310	7.199	8.020	7.999	6.510	6.361	6.690	6.759
$10_{1,0}$	9.410	8.989	8.690	8.702	10.020	9.920	11.310	11.495	8.900	8.497	9.180	9.216
$12_{1,0}$	-	11.498	-	11.878	-	12.334	-	12.879	-	10.362	-	11.985
$14_{1,0}$	-	13.302	-	14.522	-	15.073	-	15.591	-	12.640	-	14.759
β_1												
$0_{2,1}$	2.350	3.009	-	2.569	3.670	3.678	-	4.462	2.820	3.000	3.470	3.492
$2_{2,1}$	3.860	4.301	4.230	4.233	-	5.127	-	5.902	3.950	4.203	4.510	4.608
$4_{2,1}$	-	6.289	5.810	5.921	-	7.443	-	8.285	5.310	5.899	-	6.792
$6_{2,1}$	-	8.691	-	8.009	-	10.001	-	11.099	-	7.958	-	9.172
$8_{2,1}$	-	11.319	-	11.101	-	12.519	-	14.532	-	10.739	-	11.829
β_2												
$0_{3,2}$	-	7.437	-	6.589	-	8.388	-	10.099	-	6.664	-	7.722
$2_{3,2}$	-	9.000	-	8.202	-	10.200	-	11.811	-	8.007	-	9.402
$4_{3,2}$	-	11.009	-	10.341	-	12.049	-	12.972	-	10.229	-	11.538
β_0		1.464		0.963	-	2.121		1.830		1.221		1.494
σ		0.569		0.310	-	0.422		0.276		0.481		0.295

	^{124}Xe Exp	^{124}Xe Theor	^{126}Xe Exp	^{126}Xe Theor	^{148}Nd Exp	^{148}Nd Theor	^{184}Pt Exp	^{184}Pt Theor	^{186}Pt Exp	^{186}Pt Theor	^{188}Pt Exp	^{188}Pt Theor
gsb												
$4_{1,0}$	2.480	2.498	2.420	2.463	2.490	2.500	2.670	2.721	2.560	2.567	2.530	2.890
$6_{1,0}$	4.370	4.418	4.210	4.291	4.240	4.187	4.900	5.001	4.580	4.399	4.460	4.503
$8_{1,0}$	6.580	6.596	6.270	6.325	6.150	6.007	7.550	7.679	7.010	6.768	6.710	6.666
$10_{1,0}$	8.960	8.726	8.640	8.382	8.190	7.986	10.470	10.585	9.700	8.863	9.180	8.969
$12_{1,0}$	-	11.998	-	10.479	-	9.769	-	12.807	-	11.999	-	11.378
$14_{1,0}$	-	15.079	-	12.681	-	11.246	-	15.367	-	14.875	-	14.242
β_1												
$0_{2,1}$	3.580	3.402	3.380	3.201	3.040	3.082	3.020	3.546	2.460	2.798	3.010	3.209
$2_{2,1}$	4.600	4.498	4.320	4.241	3.880	4.006	5.180	5.452	4.170	4.381	4.200	4.397
$4_{2,1}$	5.690	6.289	5.250	5.862	5.320	5.589	7.570	7.943	6.380	6.599	-	6.583
$6_{2,1}$	-	8.564	-	7.828	7.120	7.411	11.040	11.157	8.360	8.581	-	8.603
$8_{2,1}$	-	11.900	-	10.062	-	9.752	-	14.601	-	12.007	-	12.100
β_2												
$0_{3,2}$	-	7.334	-	6.759	-	6.249	-	10.122	-	7.389	-	7.603
$2_{3,2}$	-	8.888	-	8.009	-	7.442	-	11.900	-	8.942	-	9.162
$4_{3,2}$	-	10.022	-	9.287	-	9.051	-	12.998	-	10.208	-	10.441
β_0		1.101	-	0.949		1.111		2.639		1.469		4.950
σ		0.279	-	0.299		0.347		0.475		0.600		0.729

Table 7: The $B(E2)$ transition rates of the $X(3)$ model at $\beta_0 = 0, 1, 2, \infty$ and its values obtained at $\beta_{0,max}$ peculiar to each angular momentum, normalized to the $B(E2; 2_{1,0} \to 0_{1,0}) = 100$ units are compared with the $X(3)$-IW model [1] and with the experimental data of $X(5)$ [34]. [Note: -IW denotes infinite well potential.]

$L^{(i)}_{s,n_\beta}$	$L^{(f)}_{s,n_\beta}$	$\beta_0 = 0$	$\beta_0 = 1$	$\beta_0 = 2$	$\beta_0 = \infty$	$\beta^{(i)}_{0,max} \to \beta^{(f)}_{0,max}$	$B(E2) - var$	$X(3)$-IW	^{176}Os-Exp
$2_{1,0}$	$0_{1,0}$	100.000	100.000	100.000	100.000	$\beta_0 \to \beta_0$	100.000	100.00	100.00
$4_{1,0}$	$2_{1,0}$	237.513	190.935	178.005	143.992	$0.844 \to \beta_0$	189.495	189.90	193.00
$6_{1,0}$	$4_{1,0}$	380.702	286.006	270.996	167.292	$1.576 \to 0.844$	250.995	248.90	267.00
$8_{1,0}$	$6_{1,0}$	523.695	384.599	369.090	185.328	$2.033 \to 1.576$	293.038	291.40	297.00
$10_{1,0}$	$8_{1,0}$	667.003	486.036	469.991	202.099	$2.143 \to 2.033$	324.599	323.80	352.50
$12_{1,0}$	$10_{1,0}$	810.954	587.658	559.744	229.986	$2.695 \to 2.143$	350.710	349.50	-
$14_{1,0}$	$12_{1,0}$	954.746	690.364	671.484	253.007	$3.643 \to 2.695$	371.992	370.70	-
$2_{2,1}$	$0_{2,1}$	166.813	160.292	152.428	69.929	$2.011 \to 0.815$	78.922	80.60	-
$4_{2,1}$	$2_{2,1}$	320.619	260.000	243.186	123.888	$3.729 \to 2.101$	139.471	140.10	-
$6_{2,1}$	$4_{2,1}$	470.001	355.240	343.376	156.031	$5.213 \to 3.729$	181.730	182.40	-
$8_{2,1}$	$6_{2,1}$	617.075	456.792	439.962	189.542	$6.098 \to 5.213$	213.899	215.50	-
$10_{2,1}$	$8_{2,1}$	763.927	557.317	542.129	215.763	$6.855 \to 6.098$	242.026	242.40	-
$12_{2,1}$	$10_{2,1}$	899.983	656.999	639.677	233.499	$8.106 \to 6.855$	268.543	265.10	-
$14_{2,1}$	$12_{2,1}$	1009.079	759.642	736.660	251.643	$9.441 \to 8.106$	281.320	-	-
$2_{3,2}$	$0_{3,2}$	233.504	221.942	209.888	56.684	$4.497 \to 2.524$	72.090	73.50	-
$4_{3,2}$	$2_{3,2}$	401.982	327.461	311.072	82.831	$6.523 \to 4.497$	118.990	120.50	-
$6_{3,2}$	$4_{3,2}$	559.801	422.880	408.564	116.085	$8.567 \to 6.523$	154.892	154.20	-
$8_{3,2}$	$6_{3,2}$	708.989	523.436	512.997	139.859	$10.438 \to 8.567$	183.019	181.20	-
$10_{3,2}$	$8_{3,2}$	858.095	624.555	609.096	166.646	$11.932 \to 10.438$	202.222	-	-
$12_{3,2}$	$10_{3,2}$	1003.933	727.909	715.990	182.910	$13.011 \to 11.932$	218.753	-	-
$14_{3,2}$	$12_{3,2}$	1151.239	832.003	819.115	202.421	$14.629 \to 13.011$	229.986	-	-

Secondly, the exact relationship between the $\nu^{X(3)}$ and the $\nu^{X(5)}$ stated in Eq.(28) does not reflect in the exact comparison of their energy levels. That is, it can be inferred from the results that

$$\epsilon^{X(3)}(\beta_0 = c + 2) \neq \epsilon^{X(5)}(\beta_0 = c), \tag{29}$$

because the total energy of the $X(5)$ contains the γ-part solutions. However, the relation

$$\epsilon_{gs,L} = 2 + \epsilon_{\beta_1,L} = 4 + \epsilon_{\beta_2,L}, \tag{30}$$

holds in all the levels for both $X(3)$ and the β-part of $X(5)$: this third remark is shown in the Table 2.

Another significant remark is such that, the values of ν, for the case of $X(5)$ at $L = 2$, correspond to those of $X(3)$, at $L = 0$. This is shown in Table 1. and the visual comparison is shown with the lines in Figure 1(b). Analytically, the behaviour of the energies of the $X(5)$ and the $X(3)$ at constant value of variation parameter, β_0, is shown in the Figure 1(a). The critical orders, $\nu(L, \beta_0)$, of the $X(5)$ and that of the $X(3)$, which define their energy levels, are plotted against the variation parameter, β_0, at constant angular momenta and shown in the Figure 1(b): it is shown, with the numerical values of ν, in the Table 1., that

$$\nu^{X(5)}(L = 0) = \nu^{X(3)}(L = 2) \quad \forall \quad \beta_0. \tag{31}$$

The derivatives of ν with respect to the β_0 are shown in Figures 2(a) and 2(b). The first and the second derivatives are carried out in order to show the stationary properties of β_0 and the values of β_0 at which the energy is minimum.

The variation of the ratio $\frac{\epsilon_{s,L}}{\epsilon_{1,2}}$ with respect to the variation parameter, β_0, for both $X(3)$ and $X(5)$ are respectively shown in the Figures 3(a) and 3(b). For all values of β_0, its values increase at $L = 0$, are constant at $L = 2$, that is $\frac{\epsilon_{s,L}}{\epsilon_{1,2}}$=1 and decrease at $L > 2$.

The ground state bands (gsb) are defined with $s = 1$; $n_\beta = 0$. The quasi-β_1 bands and the quasi-β_2 bands are defined by $s = 2$; $n_\beta = 1$ and $s = 3$; $n_\beta = 2$ respectively. The γ bands do not exist for $X(3)$ model because, $\gamma^0 = 0$. The increase in the angular momentum, L, at constant value of β_0, increases the energies, in all energy levels. Also, at constant values of the angular momentum, the increase in the β_0 increases the energy levels. The Table 2. shows the numerical solutions of Eq.(13) obtained for the ground states and the β-bands at $\beta_0 = 2, 3, 4$ and at $\beta_0 = 15$. The Figure 4(a) shows the comparison, in the $R_{4/2}$, of the $X(3)$ with $X(5)$ at $\beta_0 = \infty$ and at $\beta_{0,max}$ unique to each angular momentum, labelled as $X(3)-$var and $X(5)-$var respectively. The comparison in the $R_{0/2}$ of the $X(3)$ with $X(5)$, at $\beta_0 = \infty$ and at different values of the $\beta_{0,max}$ peculiar to each angular momentum, labelled as $X(3)-$var and $X(5)-$var respectively is shown in Figure 4(b).

The 'nature' of critical point symmetry transitions for different isotopes, constrained to one-parameter potentials, can be investigated using a variational technique. This technique was used in ref. [11] to retrieve the $U(5)$ and $O(6)$ ground state bands from the $E(5)$ within the domain of the one-parameter inverse square potential. The technique has also been used in ref. [12] and employed in ref. [16] to construct 'image' of the $X(5)$ critical symmetry and to construct the $Z(5)$ critical symmetry respectively. The forward variation of the 'control parameter', β_0, causes the nuclei transition from $X(5)$ to $SU(3)$ (i.e. $X(5) \longrightarrow SU(3)$ transition symmetry). The nature of the critical symmetry or the nuclear shape phase region under investigation predicts the directions of the variation: whether forward variation or backward variation, and also depends on the potential's boundary conditions. The rate of change of $R_{L/2}(\beta_0)$ is maximized for each L by using this approach. As shown in Table 3., each angular momentum is considered and treated separately in terms of the variation parameter, β_0, as the critical values of $R_{L/2}$ are distinct. Each value of β_0 implies a distinct potential with which the energy is maximized. The method is comparable to the "normal" variational principle used in some quantum books, in which trial wave functions are chosen and energy is minimized.

The comparisons of the ground state spectra ratios, defined in Eq.(15) with the $X(5)$ model [11], at different values of β_0 corresponds to the potentials are displayed in Figures 5(a) and 5(b) and also shown in Table 3: the visual comparison is shown in Figures 6(a), 6(b) and 6(c). It can be observed that the solutions of $X(3)(\beta_0 = \infty) \approx X(5)(\beta_0 = \infty)$. The forward variation of β_0 shifts the solutions to $X(3)$. The solutions leave $X(3)$ and approach $SU(3)$ as β_0 tends to ∞. The available experimental data of ^{162}Dy [17], which is a typical $SU(3)$ candidate are placed for comparison in Figure 6(a) and Figure 6(b). This is another remark that isotopes which have $X(3)$ signatures must lie between $U(5) \longrightarrow SU(3)$ symmetrical plane.
The two other important relations that can be deduced from the comparison are:

$$R_{L/2}(gsb) = 2 + R_{L/2}(\beta_1) = 4 + R_{L/2}(\beta_2), \tag{32}$$

at $\beta_0 = 0$ as shown numerically in the Table 3. and Table 4. This is an observable effect or a signature from Eq.(30) while the effect of Eq.(28) is observed in the spectral ratios of $X(3)$ and $X(5)$ such that

$$R_{L/2}^{X(3)}(\beta_0 = c + 2) = R_{L/2}^{X(5)}(\beta_0 = c): \quad c = 0, 1, 2, ... \tag{33}$$

In order to obtained the exact solutions of $R_{L/2}$ ratios rather than vary β_0, the technique of optimizing β_0 employed in refs. [11,12,15,16] and others has been used to obtained the solutions of $R_{L/2}$ at certain values of the β_0 peculiar to the angular momenta. These special values of β_0 are labelled $\beta_{0,max}$ and they produce exact solutions labelled $X(3)$-var, shown in Table 5. The values obtained at different values of $\beta_{0,max}$, are compared with $X(3)$-IW solutions. For all $\beta_{0,max}$, $0_{0,0}$ and $2_{0,0}$ levels yield 0.000 and 1.000 respectively. $\beta_{0,max}$ increases with increase in the angular momentum and its values are obtained at the points where the increases in β_0 become steep. $\frac{d}{d\beta_0} R_{L/2}|_{\beta_0=max}$ is achieved via a numerical procedure as $\frac{d^2}{d\beta_0^2} R_{L/2}$ vanished. The $R_{L/2}$ ratios for the ground state and the quasi-β_1 bands of the $X(3)$ and the $X(5)$ models of inverse square potentials obtained at different values of $\beta_{0,max}$, labeled $X(3)$-var and $X(5)$-var, are compared with the experimental data of ^{172,176,178,180}Os [18-21] chain, as shown in Figures 7(a) and 7(b). The ground state solutions of the $X(3)$ for $L = 0$ up to $L = 10$ are in good agreement with ^{172}Os while those of $X(5)$ are seen lying closer to ^{176}Os than ^{178}Os and ^{180}Os: the generalized comparison is moderate in the first excited state. This suggests that ^{172}Os is a good candidate for $X(3)$ model while ^{176}Os shows a signature of $X(5)$ model.
The $R_{L/2}$ theoretical predictions of the $X(3)$ model are compared with the experimental data of some selected isotopes: ^{102}Mo [22], $^{104-108}$Ru [23-25], $^{120-126}$Xe [26-29], ^{148}Nd [30] and $^{184-188}$Pt [31-33] as shown in Table 6. Each energy level is normalized to the particular $2_{0,0}$ state. The energy obtained in Eq.(13) is fitted with the experimental energy of each of the isotopes considered. The equivalent values of the β_0 for the isotopes are recorded. The quality factor, σ, used is obtained from

$$\sigma = \sqrt{\frac{\sum_i^m [(R_{s,L})_i^{Exp} - (R_{s,L})_i^{Theor}]^2}{m-1}}, \tag{34}$$

where m is the number of available experimental states, $(R_{s,L})_i^{Exp}$ and $(R_{s,L})_i^{Theor}$ represent the experimental and the theoretical spectral ratios of the ith levels normalized to the ground state with $L = 2$, $s = 1$ and $n_\beta = 0$ respectively.
Against the neutron numbers, N, of the chains of the isotopes: $^{104-108}$Ru, $^{120-126}$Xe, $^{184-188}$Pt, $^{172-180}$Os, considered for the comparison, the neutron-β_0 distribution, showing the relative positions of the isotopes, is shown in the Figure 8.
The comparison in the ground state, the quasi-β_1 bands and the quasi-β_2 bands of the $B(E2)$ transition probabilities at $\beta_0 = 0, 1, 2$ and $\beta_0 = \infty$, normalized to the $B(E2 : 2_{1,0} \to 0_{1,0}) = 100$ units with the $X(3)$-IW [1] and experimental data on $X(5)$ [34] are presented in the Table 7. The values of $\beta_{0,max}$ peculiar to each angular momentum, obtained from the optimization of β_0, in

Table 5., are employed to compute the optimized $B(E2)$ transition probabilities, labelled $B(E2)$-var. The visuals of these comparisons are shown in the Figures 9(a), 9(b) and 9(c). In order to show the nature of the solutions along the $X(5) \longrightarrow SU(3)$ symmetry region, the experimental data on the ^{158}Gd [35], which is a typical $SU(3)$ candidate, are placed for comparison in Figures 9(a) and 9(b): the solutions at $\beta_0 \to \infty$ are seen lying close to the ^{158}Gd [35]. The values of the $B(E2)$ transition probabilities decrease as the variation parameter, β_0, increases: they increase as the angular momentum increases. The forward variation, as the β_0 increases, pushes the solutions to $X(5)$ and the solutions tend to the $SU(3)$ as β_0 tends to ∞.

5 Conclusion

The $X(3)$ solutions of the Bohr Hamiltonian are obtained by solving the radial function of the Hamiltonian with an inverse square potential with the aid of MAPLE software. Analytically, an expression for the energy levels is determined from the zeros of the Bessel functions. Through the use of the variational approach and the optimization procedure, the spectra ratios and the $B(E2)$ transition probabilities are computed. The analytical solutions of the $X(3)$ model are compared with the $X(5)$ model of the inverse square potentials. It is worth noting that, $X(3)$ model is another "window" through which $X(5)$ and $SU(3)$ "pictures" can be seen: $X(3)$ lies between $U(5)$ and $SU(3)$, hence, $X(5)$ lies between $X(3)$ and $SU(3)$. It has been shown via variational procedure, that the solutions shift to $X(5)$ from $X(3)$ and approach $SU(3)$ as the variation parameter shifts forward.
The theoretical predictions on $R_{L/2}$ and $B(E2)$ with the experimental data for some selected isotopes are found to be proficient in the *gsb* and moderate in other levels. This is shown as the theoretical deviations from the experiments are quite small.
The same manner in which the Davidson potential is employed in ref. [4], the employment of the one parameter-dependent inverse square potential in the form of Eq.(1), its properties, is efficient in the variational procedure. Eq.(1) is also a good choice of potential which can be employed for the description of the nuclei transition at the critical points. For the comparison of $X(3)$ and $X(5)$ models of Bohr Hamiltonian, with the same formalism employed in this work, it is expected that Equations (28), (29), (30), (31), (32) and (33) should hold in any one-parameter-dependent potential domain such as Kratzer potential, Davidson potential and others.

Data availability statement

All the sources of data included in this article for comparison purpose, are cited and referenced accordingly, in the article.

Funding Information

No funding of any form is received for the course of this work.

References

[1] Bonatsos, D., Lenis, D., Petrellis, D. and Terziev, P.A. and Yigitoglu, I. (2006). Physics Letters B, 632, 238-242. doi: http://dx.doi.org/10.1016/j.physletb.2005.10.060

[2] Budaca, R. (2014). Physics Letters B, **739**, 56-61. doi: http://dx.doi.org/10.1016/j.physletb.2014.10.031

[3] Alimohammadi, M. and Hassanabadi, H. (2017). International Journal of Modern Physics E. **26**(9), 1750054. doi: http://dx.doi.org/10.1142/S0218301317500549

[4] Yigitoglu, I. and Gokbulut, M. (2017). Eur. Phys. J. Plus, **132**, 345.
doi: http://dx.doi.org/10.1140/epjp/i2017-11609-3

[5] Iachello, F. (2001). Phys. Rev. Lett., **87**(5), 052502.
doi: http://dx.doi.org/10.1103/PhysRevLett.87.052502

[6] Bohr, A. (1952). *The Coupling of Nuclear Surface Oscillations to the motion of individual Nucleons.* Dan. Mat . Fys. Medd . **26**(14).
url: http://www.xuantianlinyu.com.cn/Jabref/RefPdf/Bohr1952pp.pdf

[7] Bohr, A. and and Mottelson, B. (1953). Phys. Rev. **90**(4), 717.
doi: https://doi.org/10.1103/PhysRev.90.717.2

[8] Bohr, A. and Mottelson, B. (1953). *Collective and individual-particle aspects of nuclear structure.* Mat-Fys. Medd. **27**(16). 1-174.
url: https://cds.cern.ch/record/213298/files/p1.pdf

[9] Bohr, A. and Mottelson, B. (1975). *Nuclear Structure and Nuclear Deformations.* W. A. Benjamin, Inc., Reading, Massachusetts, **748**, 37-50.

[10] Iachello, F. (2000). Phys. Rev. Lett., **85**(17), 3580. doi: https://doi.org/10.1103/PhysRevLett.85.3580

[11] Ajulo, K.R., Oyewumi, K.J., Oyun, O.S. and Ajibade, S.O. (2021). Eur. Phys. J. Plus, 136(500). doi: https://doi.org/10.1140/epjp/s13360-021-01451-7

[12] Ajulo, K.R., Oyewumi, K.J., Oyun, O.S. and Ajibade, S.O. (2022). Eur. Phys. J. Plus **137**(90). doi: https://doi.org/10.1140/epjp/s13360-021-02276-0

[13] Abramowitz, M. and Stegun, I.A. (1965). *Handbook of Mathematical Functions.* Dover, New York.

[14] Gradshteyn, I.S. and Ryzhik, I.M. (1980). *Table of Integral Series and Products.* Academic, New York.

[15] Bonatsos, D., Lenis, D., Minkov, N., Raychev, P.P. and Terziev, P.A. (2003). Physics Letter B, 584, 1-2. doi: https://doi.org/10.1016/j.physletb.2004.01.018

[16] Ajulo, K.R. and Oyewumi, K.J. (2022). Physica Scripta, **137**(90). doi: https://doi.org/10.1088/1402-4896/ac76ed

[17] Helmer, R.G. (1985). Nucl. Data Sheets, **44**(4), 661-781. doi: https://doi.org/10.1016/S0090-3752(85)80054-5

[18] Greenwood, L.R. (1975). Nucl. Data Sheets, 15, 497. doi: https://doi.org/10.1016/S0090-3752(87)80023-6

[19] Horen, D.J. and B. Harmatz, B. (1976). Nucl. Data Sheets, 19, 383. doi: https://doi.org/10.1016/S0090-3752(76)80067-1

[20] Browne, E. (1988). Nucl. Data Sheets, 54, 199. doi: https://doi.org/10.1016/S0090-3752(88)80132-7

[21] Wu, S.C. and Niu, H. (2003). Nucl. Data Sheets, **100**(4), 483-705.
doi: https://doi.org/10.1006/ndsh.2003.0018

[22] DE Frenne, D. (2009). Nucl. Data Sheets, **110**(8), 1745-1915.
doi: https://doi.org/10.1016/j.nds.2009.06.002

[23] Blachot, J. (2007). Nucl. Data Sheets, **108**(10), 2035-2172. doi: https://doi.org/10.1016/j.nds.2007.09.001

[24] DE Frenne, D. and Negret, A. (2008). Nucl. Data Sheets, **109**(4), 943-1102. doi: https://doi.org/10.1016/j.nds.2008.03.002

[25] Blachot, J. (2000). Nucl. Data Sheets, **91**(2), 135-296. doi: https://doi.org/10.1006/ndsh.2000.0017

[26] Kitao, K., Tendow, Y. and Hashizume, A. (2002). Nucl. Data Sheets, **96**(2), 241-390. doi: https://doi.org/10.1006/ndsh.2002.0012

[27] Tamura, T. (2007). Nucl. Data Sheets, **108**(3), 455-632. doi: https://doi.org/10.1016/j.nds.2007.02.001

[28] Katakura, J. and Wu, Z.D. (2008). Nucl. Data Sheets, **109**(7), 1655-1877. doi: https://doi.org/10.1016/j.nds.2008.06.001

[29] Limura, H., Katakura, J. and Ohya, S. (2022). Nucl. Data Sheets, 180, 1-413. doi: https://doi.org/10.1016/j.nds.2022.02.001

[30] Nica, N. (2014). Nucl. Data Sheets 117, 1-229. doi: https://doi.org/10.1016/j.nds.2014.02.001

[31] Baglin, C.M. (2010). Nucl. Data Sheets, **111**(2), 275-523. doi: https://doi.org/10.1016/j.nds.2010.01.001

[32] Baglin, C.M. (2003). Nucl. Data Sheets, **99**(9), 1-196. doi: https://doi.org/10.1006/ndsh.2003.0007

[33] Singh, B. (2002). Nucl. Data Sheets, **95**(2), 387-541. doi: https://doi.org/10.1006/ndsh.2002.0005

[34] Melon, B. (2011). *Investigation of the $X(5)$-Structure in ^{176}Os Using Absolute Transition Probabilities.* PhD thesis, Universität zu Köln. URL: http://kups.ub.uni-koeln.de/id/eprint/4370

[35] Helmer, R.G. (2004). Nucl. Data Sheets, **101**(3), 325-519. doi: https://doi.org/10.1016/j.nds.2004.02.001